

Cascade Detector Analysis and Application to Biomedical Microscopy

Thomas L. Athey, Shashata Sawmya, and Nir Shavit

MIT CSAIL, Cambridge, MA, USA
 {tathey_1,shashata,shanir}@mit.edu

Abstract. As both computer vision models and biomedical datasets grow in size, there is an increasing need for efficient inference algorithms. We utilize cascade detectors to efficiently identify sparse objects in multiresolution images. Given an object’s prevalence and a set of detectors at different resolutions with known accuracies, we derive the accuracy, and expected number of classifier calls by a cascade detector. These results generalize across number of dimensions and number of cascade levels. Finally, we compare one- and two-level detectors in fluorescent cell detection, organelle segmentation, and tissue segmentation across various microscopy modalities. We show that the multi-level detector achieves comparable performance in 30-75% less time. Our work is compatible with a variety of computer vision models and data domains.

Keywords: Segmentation · Cascade · Microscopy

1 Introduction

Image data has driven significant discoveries in many disciplines including biology, earth sciences, and medicine. The dimensionality of images is incredible – the number of pixels in an image of a complete mouse brain can be of the same magnitude as the number of stars in the Milky Way. As image acquisition accelerates in research, with some datasets at the petabyte scale [20], there is an increasing need to design algorithms that can process images efficiently.

This work is motivated by the observation of two themes in biomedical image analysis. The first is object sparsity, such as sparse neuron labeling in brain mapping [24, 14], cell sparsity in liquid based cytology [10] and hemorrhage sparsity in CT scans [16]. The second theme is that large images are often stored at multiple resolutions [9, 12, 5, 23]. Thus, cascade detectors, which use low-resolution information to quickly rule out background regions, are a natural choice for biomedical image analysis (Fig. 1). In this work, we show how a cascade detector model can offer comparable accuracy in less time than a detector that operates only on the highest resolution. While previous work has focused on two-dimensional images and a fixed number of cascade levels, we extend these results across domain dimensionality and the cascade level number. We demonstrate this speedup in cell body (soma) detection in fluorescence imaging, organelle segmentation in electron microscopy (EM), and tissue segmentation in digital pathology. This is,

to our knowledge, the most broad application of cascade detectors to biomedical microscopy. This work could be combined with other efficient inference methods such as network sparsification and quantization to further accelerate image analysis.

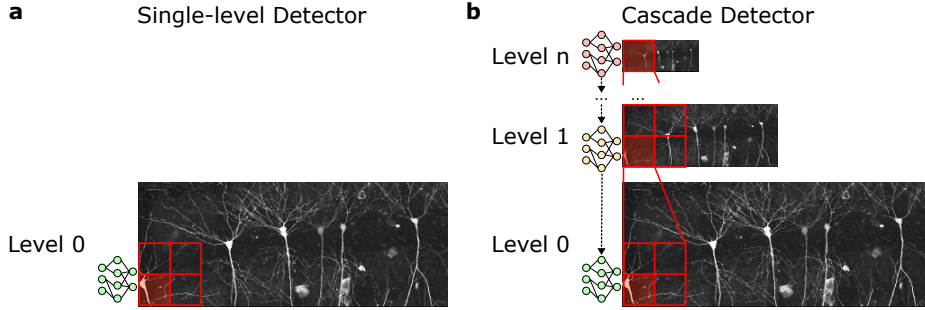


Fig. 1. Cascade detectors use different levels of a multiresolution image pyramid during inference. **a)** Schematic of a single-level detector in microscopy where a large image is broken into chunks due to memory limitations. **b)** In a cascade detector, low resolution data is processed first to rapidly rule out background regions. Lower level detectors are only called on positive candidates. Pictured is a subset of the fluorescence microscopy dataset from Bloss et al. [3].

2 Related Works

The subject of this work is performing some computer vision task such as image segmentation or object detection on a large, multiresolution image. Usually the imaging system acquired the highest resolution data, and lower resolutions were computed via some downsampling operation [9]. In order to avoid possible information loss, computer vision algorithms such as neural networks are often applied to the highest resolution. Additionally, the high resolution data is often broken into chunks due to memory limitations. The goal of our work is how to navigate through the chunks of data to efficiently accomplish a computer vision task. In this way, our work can be connected to active sensing [21].

Our approach is inspired more directly by the work of Viola and Jones [22] which introduces the concept of a classifier cascade and applies them to face detection. Subsequent theoretical work described how to train these systems optimally and how to estimate generalization performance [4]. Neural networks were then used in a cascade framework, again to detect faces [13]. The term “cascade” has also been used in other contexts such as the application of attention to multi-scale features [17], or the splitting of feature maps across attention heads [15].

3 Theoretical Motivation

We analyze a setup that is common in contemporary neuroscience research, a three dimensional image provided at multiple resolutions, with a relative down-sampling factor of two. Specifically, we consider two resolutions where the high resolution is called level 0 (L0) and the low resolution is called level 1 (L1). For simplicity, we assume that the images at both levels are decomposed into a whole number of uniformly sized chunks. Say the number of L0 chunks is n . Further, we assume that the L0 image has exactly twice as many pixels along every axis and thus there are $\frac{n}{8}$ chunks in the L1 image. The ultimate goal is to determine which L0 chunks contain some object of interest.

We consider two detector systems. The first is a traditional, single-level detector which classifies all n L0 chunks (Fig. 1a). The second is a cascade detector which is composed of both a L1 and L0 classifier. The cascade detector classifies all $\frac{n}{8}$ L1 chunks. If a L1 chunk is predicted to be positive, the associated L0 chunks are passed to the L0 detector (Fig. 1b). Thus, a positive prediction at both levels is necessary for a L0 chunk to be predicted as positive.

Say that the true labels of the L0 chunks are independent Bernoulli random variables with probability p . Further, say the predictions by the different classifiers are independent of each other when conditioned the true chunk labels. The true positive rate (TPR) and false positive rate (FPR) of the classifier at level k will be denoted β_k and α_k respectively. The single-level detector has TPR and FPR β_0 and α_0 by definition. Further,

Proposition 1. *Under the setting described above, the two level cascade detector has true positive rate $\beta_{1,0}$ and false positive rate $\alpha_{1,0}$, where*

$$\beta_{1,0} = \beta_1 \beta_0 \quad (1)$$

$$\alpha_{1,0} = (1 - p)^7 (\alpha_1 \alpha_0) + (1 - (1 - p)^7) (\beta_1 \alpha_0) \quad (2)$$

Additionally, if K_n is the number of calls to the L0 classifier, then

$$E[K_n] = (\beta_1 + (1 - p)^8 (\alpha_1 - \beta_1)) n \quad (3)$$

Proof. The first two equations follow from Bayes rule. A true positive occurs when both the L1 and L0 chunks are correctly predicted to be positive which happens with probability $\beta_1 \beta_0$.

The term $(1 - p)^7$ is the probability that all seven other L0 chunks contained within the L1 chunk are negative. In this case, $\alpha_1 \alpha_0$ is the probability that both detectors give false positives. Under the complement event, $\beta_1 \alpha_0$ represents the probability that the L1 prediction is a true positive and the L0 prediction is a false positive.

For the third equation, we assumed that the volume can be split into a whole number of chunks, so we only need to consider the case of a single L1 chunk,

then scale the result accordingly. We use the law of total expectation over the intermediate event of whether at least one of the L0 chunks is positive:

$$E[K_8] = (1 - p)^8(8\alpha_1) + (1 - (1 - p)^8)(8\beta_1) \quad (4)$$

Finally, we divide by 8 to normalize for the number of L0 subvolumes.

Figure 2 shows the dependence of these equations on various parameters.

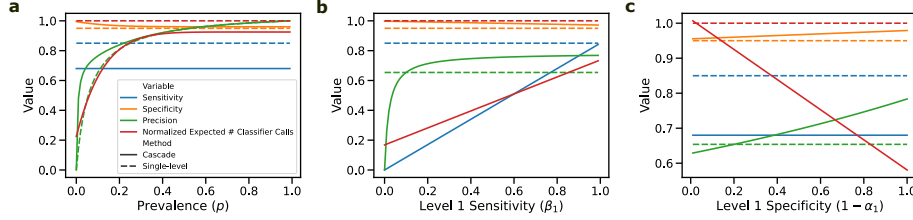


Fig. 2. The performance of the cascade detector depends on the accuracies of the detectors at both levels, and the prevalence of the object of interest. We performed a sensitivity analysis of these parameters by setting them to a set of values ($\beta_0 = 0.85$, $\beta_1 = 0.8$, $\alpha_0 = 0.05$, $\alpha_1 = 0.1$, $0 = 0.1$), then individually varying p (b), β_1 (c) and $1 - \alpha_1$ (d). The detectors’ sensitivity, specificity, precision, and expected number of calls to any classifier (normalized by the number of L0 chunks) are plotted.

It is trivial to extend these results in the following ways:

Remark 1. Proposition 1 can be extended to signals over d dimensions by replacing the exponents with $2^d - 1$ and 2^d respectively.

Remark 2. The formulas for sensitivity and specificity can be extended to cascade detectors with more than two levels by using Proposition 1 recursively.

4 Experiments

We applied single-level detectors, and a two-level cascade detectors to a variety of publicly available datasets. In each case, the L0 detector in the cascade method is identical to the single-level detector.

4.1 Datasets

Soma detection in fluorescence images The “CA1 somas” dataset is a three-dimensional fluorescence image of pyramidal neurons in mouse hippocampus [3]. Seven ground truth cell bodies were manually annotated in the test set.

The “fMOST somas” dataset is a subset of an fMOST image of a whole mouse brain [26]. The train and train sets were from different hemispheres. Eighteen ground truth cell bodies were manually annotated in the test set.

Organelle segmentation in electron microscopy In this setting, the task is two-dimensional semantic segmentation of organelles in an image stack.

The “C. elegans mitochondria” dataset involved sagittal sections of the adult C. elegans head, imaged with EM and segmented for mitochondria [25]. Slices 256-319 were used for training, slices 320-335 were used for validation, and slices 0-199 were used for testing.

The “HeLa nucleus” dataset is an EM volume, along with nuclei segmentations, from the hela-3 sample in the OpenOrganelle project [8]. Slices 0-49 were used for training, slices 50-59 were used for validation, and slices 60-124 were used for testing.

Tissue segmentation in digital pathology In this setting, the task was tissue segmentation in pathology whole slide images from the CAMELYON dataset [1]. Specifically, we used test images 1-10. Further dataset details are in Table 1.

Table 1. Dataset details, including resolution and size of the train/test sets (in pixels).

Dataset	Access Portal	L0 (nm ³)	res.	L1 (nm ³)	res.	L0 Set (px.)	Train Size	L0 Test Set Size (px.)
CA1 so- mas	BossDB [9]	800 × 800 × 800		1.6e3 × 1.6e3 × 1.6e3		720 × 938 × 179		718 × 938 × 179
fMOST somas	BIL [12]	3.5e3 × 3.5e3 × 1e5		3.5e3 × 3.5e3 × 1e3		1410 × 1900 × 1000		1410 × 1900 × 1000
C. elegans mito.	BossDB [9]	16 × 16 × 30		32 × 32 × 30		4992 × 2752 × 80		4992 × 2752 × 200
HeLa nu- cleus	OpenOrganelle [8]	32 × 32 × 25.9		64 × 64 × 51.8		1500 × 1550 × 60		1500 × 1550 × 64
H&E tis- sue	CAMELYON [1]	1e3 × 1e3		2e3 × 2e3		N/A		10 images

4.2 Implementation

For soma detection in fluorescence imaging, the detectors were ilastik pixel classification modules (random forests) [2]. In EM organelle segmentation, the detectors were U-nets with pretrained ResNet backbones [19]. For tissue segmentation, we used the “HEST” pretrained model via the TRIDENT package [11, 27].

Connected components below a certain area threshold (in pixels) were filtered out after segmentation. Segmentations were converted to object detections by identifying connected components. Neural networks were executed on a GPU, and ilastik experiments were executed on a CPU. A summary of the implementation details is given in Table 2.

Table 2. Implementation details of experiments.

Dataset	Detector	L1:L0 Area Threshold (px.)	Hardware (memory)
CA1 somas	ilastik	1000:50	Apple M2 Pro (16GB)
fMOST somas	ilastik	20:5	Apple M2 Pro (16GB)
C. elegans mito.	U-Net	36:10	GeForce RTX 2080 Ti (12GB)
HeLa nucleus	U-Net	1000:250	GeForce RTX 2080 Ti (12GB)
H&E tissue	HEST	0:0	GeForce RTX 2080 Ti (12GB)

5 Results

The results are organized in Table 3. On the CA1 somas dataset, both detectors detected six out of seven cell bodies, and had no false positives (Fig. 3a). The cascade detector ran more than twice as fast as the single-level detector.

On the fMOST somas dataset, the cascade detector ran almost four times as fast, but had one more false positive and one more false negative than the single-level detector. Some of the detections are shown in Figure 3b.

The detectors had identical accuracy on the C. elegans mitochondria dataset. Mitochondria was densely present in this dataset, so the primary advantage of the cascade detector was as a tissue detector that avoided calling the L0 classifier on blank margins (Fig. 3c).

The cascade detector was over twice as fast on the HeLa nucleus dataset, with a reduction of only 0.01 in recall. Finally, the cascade detector was 40% faster on the H&E tissue dataset, and disagreed with the single-level detector on less than 1% of pixels.

Table 3. Comparison of single-level and cascade detector on five datasets. In each case, results are reported from the held-out test set. For organelle semantic segmentation, recall and precision are computed pixelwise. For the H&E dataset, accuracy is computed with respect to the single-level detector output. “L1:L0 Calls” denotes the number of calls to the level 1 or level 0 detector.

Dataset	Detector	Recall	Precision	L1:L0 Calls	Runtime (s)
CA1 somas	Single-level	0.86	1.0	0:96	837
	Cascade	0.86	1.0	12:40	386
fMOST somas	Single-level	0.61	0.85	0:1200	13484
	Cascade	0.56	0.83	400:104	3396
C. Elegans mito.	Single-level	0.81	0.55	0:44000	601
	Cascade	0.81	0.55	12000:18024	382
HeLa nucleus	Single-level	0.91	0.95	0:2688	1263
	Cascade	0.90	0.95	384:1088	569
H&E tissue	Single-level	N/A	N/A	0:38452	1749
	Cascade	>0.99	1.0	9681:11792	1043

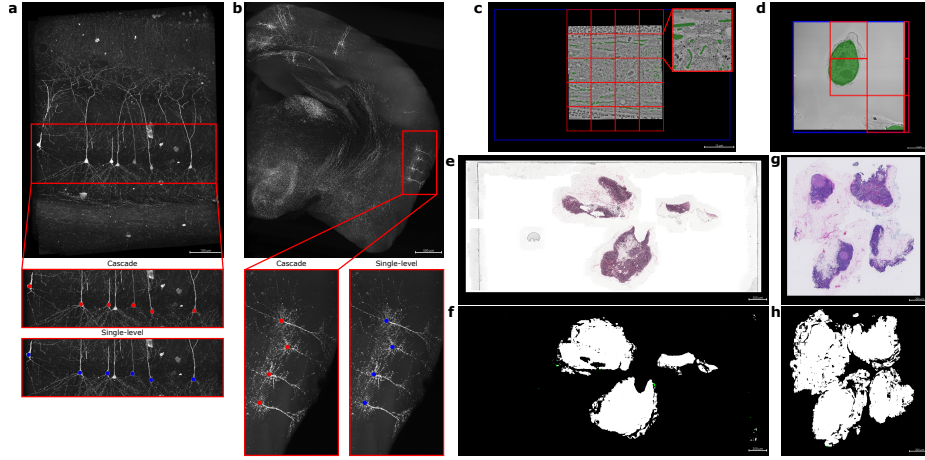


Fig. 3. A selection of results on the various datasets. **a** The test image from the CA1 somas dataset included seven fluorescent neurons [3] with insets showing the detections from the cascade detector (red points) and single-level detector (blue points). **b** The test image from the fMOST somas dataset includes fluorescent neurons throughout mouse cortex [26]. Insets show four neurons that were correctly detected by both the cascade detector (red points) and single-level detector (blue points). **c** A slice of the test image from the *C. elegans* mitochondria dataset are shown, with the ground truth segmentation overlaid in green, and the outer limits of the volume shown in blue [25]. Red grid lines depict the L1 subvolumes that were passed to the L0 detector. **d** A slice of the HeLa nucleus test set is shown, with the same overlays as in **c**. **e-h** Two test images from the H&E tissue dataset are shown (**e,g**), with the detector segmentations (**f,h**). The tissue segmentation by the single-level detector (green) and cascade detector (magenta) are summed in color space where they overlap (white).

6 Discussion

In this work we show that cascade detectors, which have been popular in face detection applications, can be successfully applied to microscopy data for tasks such as fluorescent soma detection, organelle segmentation, and tissue segmentation. Under a conditional independence assumption, we show that the number of inference calls can be dramatically reduced in the cascade setting if the object of interest is sparse. These results extend to signals on a domain of arbitrary dimension, and our experiments include both two-dimensional and three-dimensional images, and both random forest and neural network detectors.

The main limitation in our theoretical work is our assumption that the performance of detectors at different levels are independent, conditioned whether an object exists in that region. In practice, detectors at different levels might be correlated. For example, inherent difficulty of different samples might lead to correlation between the detectors. A model proposed by Eckhardt and Lee [6], and summarized by Hansen and Salamon [7] incorporates sample-dependent error rates. Our accuracy result in Proposition 1 would change by allowing all variables to depend on the sample x (e.g. β_1 becomes $\beta_1(x)$), then integrating over the probability distribution of x . We note that the number of classifier calls from Proposition 1 does not change, since it involves only the L1 detector.

Another potential concern is that constructing a cascade detector involves training detectors at different resolutions. It is theoretically possible to use the same L0 training data to train higher level detectors by downsampling the annotations, or to use a single detector that supports multiple resolutions [28, 18]. However, these approaches would likely lead to statistical dependence mentioned earlier. In practice, the decision on if and how to train detectors at various resolutions depends on the number of training samples needed, the cost of obtaining annotations, and the extent to which statistical dependence affects accuracy.

There are several potential future directions stemming from this work. The first is comparing predicted performance from Proposition 1 to actual performance. The detectors could be applied to a validation dataset to estimate the sensitivities and specificities used in the given formulas. Further, one could estimate statistical dependence between detectors in practice by computing correlations between their predictions.

The cascade method showed a larger speedup on three-dimensional images. This agrees with Remark 1 where, in the limit of increasing sparsity, the expected number of classifier calls decreases with domain dimension. We are also interested to see if this trend extends to other dimensions such as time-series data (one-dimensional), or data that varies in both space and time. Setting up a cascade detector with more than two levels is also a potential area of future work.

This work is orthogonal to other areas of research into efficient inference such as sparsification and quantization, which focus on the arithmetical implementation of neural networks. Those methods could be combined with this work to further accelerate image analysis. We believe this work has broad utility in making image analysis in microscopy data more efficient since it is agnostic to the type of detector used, the domain dimensionality, and the object of interest.

References

1. Alexi, B., Altuna, H., Babak, B.E., Wauters Carla, Geert, L., Jeroen, L.V., Dijk Van Marcory, Maschenka, B., Meyke, H., Nikolas, S., Oscar, G., Paul, D.V., Peter, B., Bult Peter, Manson Quirine, Vogels Rob, Rob, D.L.V.: Supporting data for "1399 H&E-stained sentinel lymph node sections of breast cancer patients: the CAMELYON dataset" (2018). <https://doi.org/10.5524/100439>
2. Berg, S., Kutra, D., Kroeger, T., Straehle, C.N., Kausler, B.X., Haubold, C., Schiegg, M., Ales, J., Beier, T., Rudy, M., Eren, K., Cervantes, J.I., Xu, B., Beutenmueller, F., Wolny, A., Zhang, C., Koethe, U., Hamprecht, F.A., Kreshuk, A.: Ilastik: Interactive Machine Learning for (Bio)Image Analysis. *Nature Methods* **16**(12), 1226–1232 (2019)
3. Bloss, E.B., Cembrowski, M.S., Karsh, B., Colonell, J., Fetter, R.D., Spruston, N.: Structured Dendritic Inhibition Supports Branch-Selective Integration in CA1 Pyramidal Cells. *Neuron* **89**(5), 1016–1030 (Mar 2016)
4. Brubaker, S.C., Mullin, M.D., Rehg, J.M.: Towards Optimal Training of Cascaded Detectors. In: *Computer Vision – ECCV 2006*. pp. 325–337. Springer, Berlin, Heidelberg (2006)
5. Burns, R., Roncal, W.G., Kleissas, D., Lillaney, K., Manavalan, P., Perlman, E., Berger, D.R., Bock, D.D., Chung, K., Grosenick, L., Kasthuri, N., Weiler, N.C., Deisseroth, K., Kazhdan, M., Lichtman, J., Reid, R.C., Smith, S.J., Szalay, A.S., Vogelstein, J.T., Vogelstein, R.J.: The Open Connectome Project Data Cluster: Scalable Analysis and Vision for High-Throughput Neuroscience. *Scientific and Statistical Database Management* (2013)
6. Eckhardt, D.E., Lee, L.D.: A Theoretical Basis for the Analysis of Multiversion Software Subject to Coincident Errors. *IEEE Transactions on Software Engineering* **11**(12), 1511–1517 (Dec 1985)
7. Hansen, L., Salamon, P.: Neural network ensembles. *IEEE Transactions on Pattern Analysis and Machine Intelligence* **12**(10), 993–1001 (Oct 1990)
8. Heinrich, L., Bennett, D., Ackerman, D., Park, W., Bogovic, J., Eckstein, N., Petruncio, A., Clements, J., Pang, S., Xu, C.S., Funke, J., Korff, W., Hess, H.F., Lippincott-Schwartz, J., Saalfeld, S., Weigel, A.V.: Whole-cell organelle segmentation in volume electron microscopy. *Nature* **599**(7883), 141–146 (Nov 2021)
9. Hider, R., Kleissas, D., Gion, T., Xenos, D., Matelsky, J., Pryor, D., Rodriguez, L., Johnson, E.C., Gray-Roncal, W., Wester, B.: The Brain Observatory Storage Service and Database (BossDB): A Cloud-Native Approach for Petascale Neuroscience Discovery. *Frontiers in Neuroinformatics* **16** (Feb 2022)
10. Hussain, E., Mahanta, L.B., Borah, H., Das, C.R.: Liquid based-cytology Pap smear dataset for automated multi-class diagnosis of pre-cancerous and cervical cancer lesions. *Data in Brief* **30**, 105589 (Apr 2020)
11. Jaume, G., Doucet, P., Song, A.H., Lu, M.Y., Almagro-Pérez, C., Wagner, S.J., Vaidya, A.J., Chen, R.J., Williamson, D.F.K., Kim, A., Mahmood, F.: HEST-1k: A Dataset for Spatial Transcriptomics and Histology Image Analysis. *Advances in Neural Information Processing Systems* **37** (2025)
12. Kenney, M., Vasylieva, I., Hood, G., Cao-Berg, I., Tuite, L., Laghaei, R., Smith, M.C., Watson, A.M., Ropelewski, A.J.: The Brain Image Library: A Community-Contributed Microscopy Resource for Neuroscientists. *Scientific Data* **11**(1), 1212 (Nov 2024)
13. Li, H., Lin, Z., Shen, X., Brandt, J., Hua, G.: A convolutional neural network cascade for face detection. In: *2015 IEEE Conference on Computer Vision and Pattern Recognition (CVPR)*. pp. 5325–5334. IEEE, Boston, MA, USA (Jun 2015)

14. Lin, R., Wang, R., Yuan, J., Feng, Q., Zhou, Y., Zeng, S., Ren, M., Jiang, S., Ni, H., Zhou, C., Gong, H., Luo, M.: Cell-type-specific and projection-specific brain-wide reconstruction of single neurons. *Nature Methods* **15**(12), 1033–1036 (Dec 2018)
15. Liu, S., Yue, W., Guo, Z., Wang, L.: Multi-branch CNN and grouping cascade attention for medical image classification. *Scientific Reports* **14**(1), 15013 (Jul 2024)
16. Piao, Z., Gu, Y.H., Jin, H., Yoo, S.J.: Intracerebral hemorrhage CT scan image segmentation with HarDNet based transformer. *Scientific Reports* **13**(1), 7208 (2023)
17. Rahman, M.M., Marculescu, R.: Medical Image Segmentation via Cascaded Attention Decoding. In: 2023 IEEE/CVF Winter Conference on Applications of Computer Vision (WACV). pp. 6211–6220. IEEE, Waikoloa, HI, USA (Jan 2023)
18. Ren, S., He, K., Girshick, R., Sun, J.: Faster R-CNN: Towards Real-Time Object Detection with Region Proposal Networks. In: *Advances in Neural Information Processing Systems*. vol. 28 (2015)
19. Ronneberger, O., Fischer, P., Brox, T.: U-net: Convolutional networks for biomedical image segmentation. *Medical image computing and computer-assisted intervention—MICCAI* **9351**, 234–241 (2015)
20. Shapson-Coe, A., Januszewski, M., Berger, D.R., Pope, A., Wu, Y., Blakely, T., Schalek, R.L., Li, P.H., Wang, S., Maitin-Shepard, J., Karlupia, N., Dorkenwald, S., Sjostedt, E., Leavitt, L., Lee, D., Troidl, J., Collman, F., Bailey, L., Fitzmaurice, A., Kar, R., Field, B., Wu, H., Wagner-Carena, J., Aley, D., Lau, J., Lin, Z., Wei, D., Pfister, H., Peleg, A., Jain, V., Lichtman, J.W.: A petavoxel fragment of human cerebral cortex reconstructed at nanoscale resolution. *Science* **384**(6696) (2024)
21. Varotto, L., Cenedese, A., Cavallaro, A.: Active Sensing for Search and Tracking: A Review (Dec 2021). <https://doi.org/10.48550/arXiv.2112.02381>
22. Viola, P., Jones, M.J.: Robust Real-Time Face Detection. *International Journal of Computer Vision* **57**(2), 137–154 (May 2004)
23. Wang, F., Oh, T.W., Vergara-Niedermayr, C., Kurc, T., Saltz, J.: Managing and Querying Whole Slide Images. *Proceedings of SPIE* **8319** (Feb 2012)
24. Winnubst, J., Bas, E., Ferreira, T.A., Wu, Z., Economo, M.N., Edson, P., Arthur, B.J., Bruns, C., Rokicki, K., Schauder, D., Olbris, D.J., Murphy, S.D., Ackerman, D.G., Arshadi, C., Baldwin, P., Blake, R., Elsayed, A., Hasan, M., Ramirez, D., Dos Santos, B., Weldon, M., Zafar, A., Dudman, J.T., Gerfen, C.R., Hantman, A.W., Korff, W., Sternson, S.M., Spruston, N., Svoboda, K., Chandrashekar, J.: Reconstruction of 1,000 Projection Neurons Reveals New Cell Types and Organization of Long-Range Connectivity in the Mouse Brain. *Cell* **179**(1), 268–281 (2019)
25. Witvliet, D., Mulcahy, B., Mitchell, J.K., Meirovitch, Y., Berger, D.R., Wu, Y., Liu, Y., Koh, W.X., Parvathala, R., Holmyard, D., Schalek, R.L., Shavit, N., Chisholm, A.D., Lichtman, J.W., Samuel, A.D.T., Zhen, M.: Connectomes across development reveal principles of brain maturation. *Nature* **596**(7871), 257–261 (Aug 2021)
26. Zeng, H.: Whole brain raw fMOST images from mouse: AIBS_746222364 (2024). <https://doi.org/10.35077/ace-bag-kit>
27. Zhang, A., Jaume, G., Vaidya, A., Ding, T., Mahmood, F.: Accelerating Data Processing and Benchmarking of AI Models for Pathology (Feb 2025). <https://doi.org/10.48550/arXiv.2502.06750>
28. Zhang, W., Zelinsky, G., Samaras, D.: Real-time Accurate Object Detection using Multiple Resolutions. In: 2007 IEEE 11th International Conference on Computer Vision. pp. 1–8 (Oct 2007)